# NONDESTRUCTIVE EVALUATION (NDE) OF SINTERED SILICON CARBIDE AND ITS CORRELATION TO MICROSTRUCTURE AND MECHANICAL PROPERTIES

Douglas M. Slusark, M.V. Demirbas*, Andrew Portune, Steven Miller, and Richard A. Haber
Rutgers University
Department of Materials Science and Engineering
607 Taylor Rd
Piscataway, NJ 08854

Raymond Brennan, William Green, Ernest Chin, and James Campbell
U.S. Army Research Laboratory
Aberdeen Proving Ground
2201 Aberdeen Boulevard
Aberdeen Proving Ground, MD 21005

## ABSTRACT

High density is a critical acceptance criterion for armor ceramics. Quantifying the difference in density between what would be considered to be a "good" or "bad" region is complicated. As density is reduced from theoretical, does this infer the presence of defects? The minimum acceptable density that ensures favorable ballistic performance is unknown. This question concerns not only the presence of defective regions, which may include pores or inclusions, but also the spatial distribution of the defect within the sample. This study will seek to expand upon the work of Demirbas *et al* [2,10]. in correlating the microstructural assessment, mechanical properties, and non-destructive evaluation results of ceramic armor tiles. This study will present the techniques necessary for microstructural analysis, which include nearest-neighbor distance distributions, tessellation analysis, average pore size, and pore size distributions. The ability of Knoop indentation and 4-pt flexure tests, combined with the results of ultrasound C-scans, to reliably predict ballistic performance of armor ceramics will be evaluated.

## INTRODUCTION

Ceramics possess many attributes that make them attractive materials for armor applications. These include high strength and hardness, and low relative density. The properties of a ceramic are influenced by the presence of second-phase particles, pores, and inclusions, as well as its chemical constituents. Additionally, the spatial distribution of features within the sample has an effect on the local mechanical properties as well as the mechanical integrity of the entire piece.

Microstructural assessment tools such as nearest neighbor distance distributions provide information about the spatial distribution of features[1]. Spatial distributions of pores within a material may include an evenly-distributed material that contains large or small pores, large elongated pores, isolated large pores, or clusters of pores[2].

Quasi-static mechanical testing methods such as Knoop microhardness indentation provide a means for validating the results of microstructural analysis. It is an easy and relatively inexpensive test to carry-out, and has been shown to be a good predictor of ballistic performance of a material[3]. One limitation of this method is the small volume of interaction beneath the Knoop indenter. The volume of maximum stress in a 4-pt modulus of rupture test is significantly larger and reaches much farther into the bulk of the sample, increasing the likelihood of activation of a critical flaw. Through the use of fractography to locate the flaw and the removal of material around it, it may be possible to perform hardness tests at the fracture site, thereby providing a correlation between the two methods.

Non-destructive evaluation methods such as ultrasound C-scans provide a valuable way to examine the bulk of a material. As the technology and our understanding of the method continue to improve, predicting the

# Report Documentation Page

*Form Approved*
*OMB No. 0704-0188*

Public reporting burden for the collection of information is estimated to average 1 hour per response, including the time for reviewing instructions, searching existing data sources, gathering and maintaining the data needed, and completing and reviewing the collection of information. Send comments regarding this burden estimate or any other aspect of this collection of information, including suggestions for reducing this burden, to Washington Headquarters Services, Directorate for Information Operations and Reports, 1215 Jefferson Davis Highway, Suite 1204, Arlington VA 22202-4302. Respondents should be aware that notwithstanding any other provision of law, no person shall be subject to a penalty for failing to comply with a collection of information if it does not display a currently valid OMB control number.

| 1. REPORT DATE | 2. REPORT TYPE | 3. DATES COVERED |
|---|---|---|
| **DEC 2008** | **N/A** | **-** |

| 4. TITLE AND SUBTITLE | 5a. CONTRACT NUMBER |
|---|---|
| **Nondestructive Evaluation (Nde) Of Sintered Silicon Carbide And Its Correlation To Microstructure And Mechanical Properties** | 5b. GRANT NUMBER |
| | 5c. PROGRAM ELEMENT NUMBER |
| 6. AUTHOR(S) | 5d. PROJECT NUMBER |
| | 5e. TASK NUMBER |
| | 5f. WORK UNIT NUMBER |
| 7. PERFORMING ORGANIZATION NAME(S) AND ADDRESS(ES) **Rutgers University Department of Materials Science and Engineering 607 Taylor Rd Piscataway, NJ 08854** | 8. PERFORMING ORGANIZATION REPORT NUMBER |
| 9. SPONSORING/MONITORING AGENCY NAME(S) AND ADDRESS(ES) | 10. SPONSOR/MONITOR'S ACRONYM(S) |
| | 11. SPONSOR/MONITOR'S REPORT NUMBER(S) |

12. DISTRIBUTION/AVAILABILITY STATEMENT
**Approved for public release, distribution unlimited**

13. SUPPLEMENTARY NOTES
**See also ADM002187. Proceedings of the Army Science Conference (26th) Held in Orlando, Florida on 1-4 December 2008, The original document contains color images.**

14. ABSTRACT

15. SUBJECT TERMS

| 16. SECURITY CLASSIFICATION OF: | | | 17. LIMITATION OF ABSTRACT | 18. NUMBER OF PAGES | 19a. NAME OF RESPONSIBLE PERSON |
|---|---|---|---|---|---|
| a. REPORT | b. ABSTRACT | c. THIS PAGE | | | |
| **unclassified** | **unclassified** | **unclassified** | **UU** | **8** | |

ballistic performance of an armor tile through non-destructive methods becomes possible.

## EXPERIMENTAL PROCEDURE

Three groups of SiC tiles were used in this study. Group I contained 4 commercially available sintered SiC tiles, while group II was comprised of 3 commercially available hot-pressed SiC tiles. Group III, the largest group, is made up of 41 sintered commercially available Hexoloy SiC tiles. Microstructural analysis, which included average pore size and pore size distribution, nearest-neighbor distance distribution, and tessellation analysis, was performed on the tiles in group I with the intent of quantifying the microstructure. The analysis of the tiles in group II was more comprehensive, as the techniques listed above were combined with mechanical testing and non-destructive analysis methods to determine if a correlation existed amongst the three areas. The testing regimen for the tiles in group III will combine microstructural analysis, Knoop hardness and 4-pt flexure testing, and improved ultrasound scanning methods. Ultimately, selected tiles from group C will undergo ballistic impact assessment. The goal of this study is determine if non-destructive evaluation methods can serve as a predictor of ballistic performance of armor ceramics.

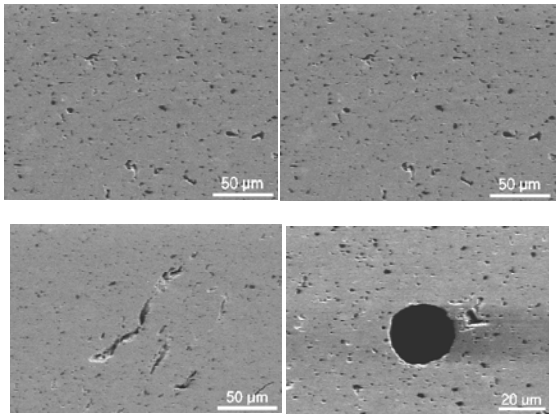


Figure 1 – Sample A, Sample B, Sample C, Sample D[2]

SEM micrographs of the tiles in group A appear in Figure 1. Image analysis was performed on the images using Image Processing Toolkit 3.0 from Reindeer Graphics.

This first step in image analysis is thresholding, where a pixel is assigned a value of 1 if the intensity of the pixel is above a certain value and 0 if it is not. A binary image is created by coloring pixels with the value of 1 black and 0 white. Closing and erosion is then done to smooth features and remove isolated pixel noise from the image. The following step is the filling of holes, which returns the intensity to the interior of a pore which may have been excluded in the thresholding operation. Finally, features that touch the edge of the image are removed to confine the analysis to features that are entirely within the field of view[4,5].

The pore size distribution and average pore size of these samples are shown in Figures 2 and 3. Sample B has the smallest average pore size, while samples C and D have the broadest distribution of pore diameters. Sample A has the largest average pore size, but a much lower standard deviation than either samples C or D.

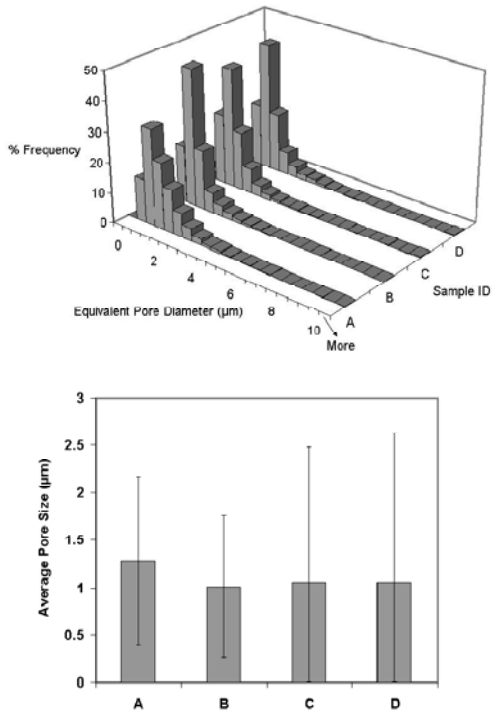


Figures 2 and 3 – Pore size distribution and average pore size of four SiC samples[2]

A more sophisticated technique is the nearest neighbor distance distribution, which provides information on the spatial distribution of pores within the microstructure rather than their relative size. The x- and y-coordinates of all pore centroids in the image were measured with Image Processing Toolkit 3.0. The distance between the pore of interest and all other pores is measured with the shortest distance being recorded. This is done for every pore in the image. The results of the distribution can be seen in Figure 4.

Samples A and B have relatively narrow distributions and correspondingly low variance values. The distributions of samples C and D are much wider and contain a considerable amount of values towards the right side of the histogram, which is indicative of an inhomogeneous microstructure[2].

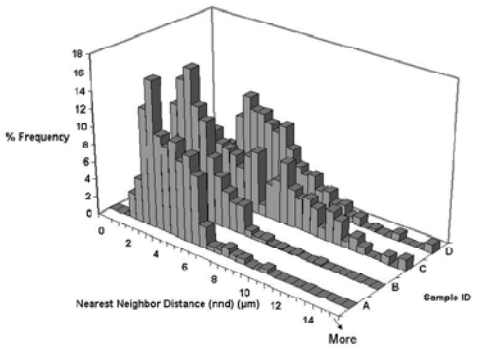


Figure 4 – Nearest Neighbor Distance Distribution of four SiC samples[2]

A method for classifying the distributions is through the use of the parameters Q and V[6]. In this use:

$$Q = \frac{\mu_o}{\mu_e} = \frac{\text{observed mean nearest-neighbor distance}}{\text{expected mean nearest-neighbor distance}}$$

$$V = \frac{var_o}{var_e} = \frac{\text{observed variance of nearest-neighbor distance}}{\text{expected variance of nearest-neighbor distance}}$$

The expected nearest-neighbor distance and variance are calculated by Image Processing Toolkit 3.0, and are for a random distribution, while the observed values are calculated from the nearest-neighbor distribution. The conditions for the classifications are: (a) random distribution, Q~1 and V~1; (b) regular distribution, Q>1 and V<1; (c) clustered distribution, Q<1 and V<1; (d) random distribution with clusters, Q<1 and V>1[6,7,8]. The results of this analysis can be seen in Table 1. All four samples have a Q value that is approximately 1. Only sample B has a V value that is near 1, while the values for the other samples are considerably higher. All four samples can be classified as having a random distribution.

Table 1 – Q and V values for Group I[2]

| Sample | Q | V |
|---|---|---|
| A | 1.154 | 3.726 |
| B | 1.155 | 1.174 |
| C | 1.059 | 5.068 |
| D | 1.104 | 4.027 |

Another type of spatial distribution analysis tool used was Tessellation analysis. This involves the construction of polygons around all features in an image. Straight lines are drawn between features, and are bisected by perpendicularly drawn lines. Polygons are formed where the perpendicular lines meet. Image Processing Toolkit 3.0 is used to determine the area of each cell. Tessellation analysis is a useful tool for determining clustering of pores, which will be indicated by a wide cell area distribution.

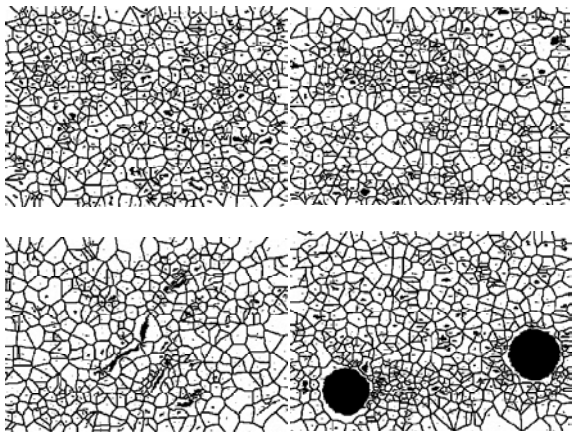

Figure 5 – Tessellations of Sample A, Sample B, Sample C, and Sample D[2]

Tessellated images of the four samples are shown in Figure 5, while Figure 6 contains the corresponding cell area distributions. Sample B has the narrowest distribution, which indicates the least amount of clustering, along with the lowest fraction of cells that are greater than 100μm$^2$ in size. This is followed next by sample A. Samples C and D have the largest fraction of cells with an area of greater than 100μm$^2$, which is indicative of clustering.

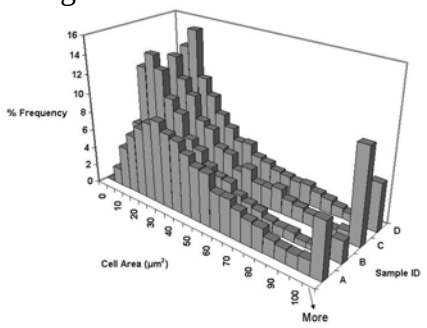


Figure 6 – Cell area distributions from tessellated images[2]

An additional method for quantifying the amount of clustering in a microstructure is the parameters $P_1$ and $P_2$, as identified by Murphy *et al*[9]. $P_1$ can be used to determine the amount of spread in a distribution as it compares the variance of a distribution to that of a random sample. $P_2$ measures the asymmetry, and will point out the presence of a tail in the distribution[9]. $P_1$ and $P_2$ values of 1 indicate a random distribution.

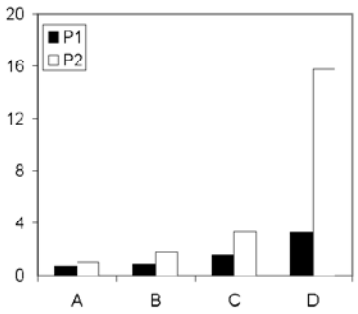


Figure 7 – $P_1$ and $P_2$ values of Group I SiC samples[2]

$P_1$ and $P_2$ values for the four samples are shown in Figure 7. Samples A and B have a $P_1$ value that is very near 1, while the value for sample C is approximately twice that. Sample D has $P_1$ and $P_2$ values of 3.28 and 15.78, respectively, which indicates that there is a greater degree of clustering in sample D then in the other samples.

The microstructural analysis techniques employed on the micrographs of the four tiles in group I did not produce consistent results for every tile through every method. However, there were identifiable trends amongst the results. Samples C and D were shown to have the widest nearest-neighbor distance and Tessellation analysis cell-area distributions, and also had the highest fraction of cells with an area greater than 100μm$^2$. These samples had the highest variance values in the Q and V analysis, and had $P_1$ and $P_2$ values that were much higher than samples A or B, with sample D in particular. Conversely, samples A and B had the narrowest nearest-neighbor distance and Tessellation cell-area distributions, and $P_1$,$P_2$,Q, and V values that were closest to 1. These results indicate that samples C and D had the most inhomogeneous and clustered microstructures, while samples A and especially B were the closest to random.

Group II was comprised of 3 hot-pressed SiC tiles. Two of the tiles were under the minimum density set by the manufacturer. Tile LD contained a low-density region, while tile DEF had a defective region that was white in color. Tile AG was accepted by the manufacturer, and will be considered the baseline tile. Knoop microhardness indentation testing was carried out on the tiles at a number of loads, and provided data for comparison to the results of the microstructural analysis. The results of these two assessments were then compared to the data obtained from ultrasound non-destructive testing that had been carried out on the tiles.

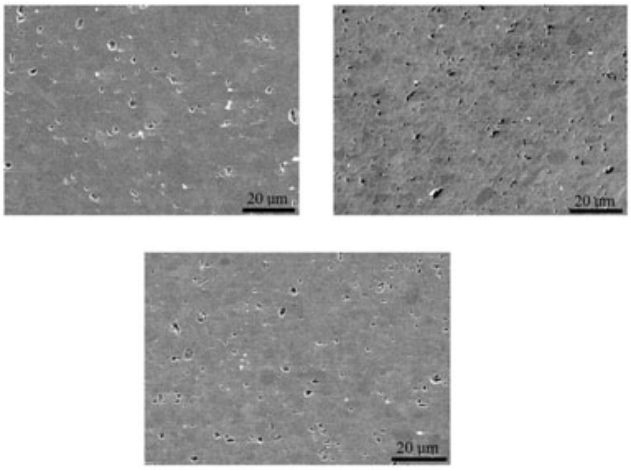


Figure 8 – SEM micrographs of hot-pressed SiC samples LD, DEF, and AG[10]

SEM micrographs of the 3 tiles can be seen in Figure 8. Image analysis was carried out on the micrographs, which included construction of nearest-neighbor distance distributions, in Figure 9. Tile LD has the widest distribution, as well as a significant number of peaks at greater than 10µm distance, which indicates an inhomogeneous microstructure. Tiles DEL and AG have significantly narrower distributions. Q and V parameters were also calculated for the distributions, as shown in Figure 10. Tile LD is shown to be in the region of a random distribution with clusters, while tiles DEF and AG do not show any clustering.

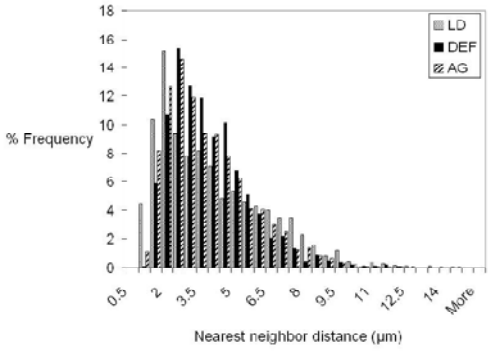


Figure 9 - Nearest-Neighbor Distance Distribution of Group II tiles[10]

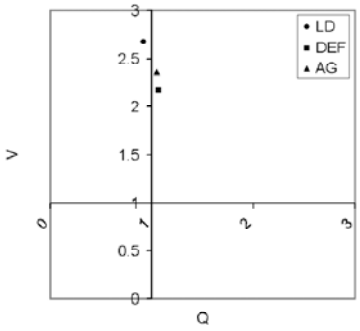


Figure 10 – Q-V plot of Group II tiles[10]

Knoop microhardness indentation testing was carried out on the 3 samples at loads of 2kg, 1kg, 500g, 300g, and 100g. 100 indentations were completed for each sample, with an indentation spacing of 0.5mm. The hardness data was processed using Weibull analysis, which can be found in Figures 11, 12, and 13.

Analysis of the Weibull plots show that there is no correlation between hardness values at different loads. For tile LD, a straight-line Weibull distribution is shown for loads of 100g and 2kg, while the other loads show a multimodal distribution. A multimodal distribution is shown for all loads for tile AG, while a straight-line distribution occurs at loads of 2kg and 500g for tile DEF. There was not any one tile that demonstrated the highest hardness value for every load.

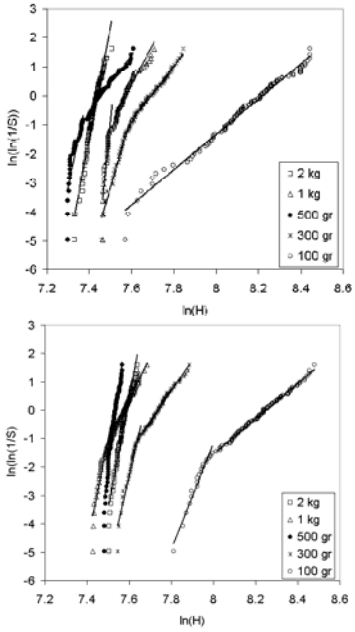

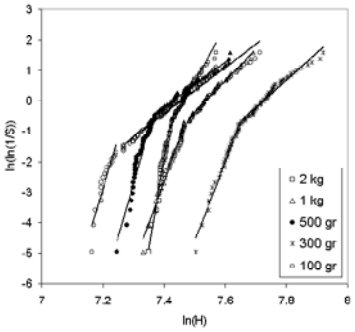


Figures 11, 12, and 13 - Weibull plots of tiles LD, DEF, and AG[10]

A correlation between the results of the microstructural analysis and hardness data is complicated by the variation in the hardness results. This can be somewhat alleviated by only taking the 2kg load into account, which is the convention when considering SiC armor plates. In this case, tile AG has the highest $m_1$ Weibull modulus of 59.5, followed by tiles DEF and LD at 38.9 and 37.8. Linearizing the distance from the random point (1,1) to the Q-V value of each tile provides a basis for comparison. The calculated distances for tiles LD, AG, and DEF are 1.69, 1.36, and 1.17, with a lower value indicating a more random microstructure. Tile LD has the lowest modulus at 2kg and the longest distance. The results for tiles AG and DEF do not match up when comparing the two methods, most likely due to the inconsistent hardness results.

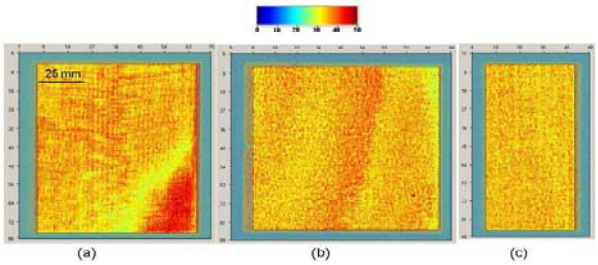


Figure 14 – 125MHz Ultrasound C-Scan images of tiles LD, DEF, and AG[10]

Ultrasound C-scan images of these tiles are shown in Figure 14. The ultrasound scans were performed with a 125MHz transducer, and are based upon the measurement of the signal amplitude from the bottom surface reflection. The scale in the image is based upon the strength of the reflected signal, in mV, at each scanning point. Tile AG has a uniform C-scan image, while a low-density area appears in the image for tile LD, and a single defect appears in the upper-right hand corner of the DEF image. The ultrasound images were processed in a manner similar to the earlier SEM micrographs, as shown in Figure 15, for microstructural assessment and a comparison to the previous data.

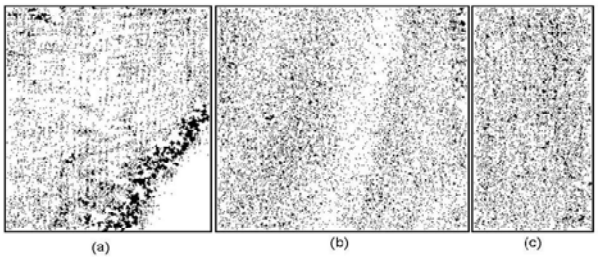


Figure 15 – Processed image of 125MHz Ultrasound image of tiles LD, DEF, and AG[10]

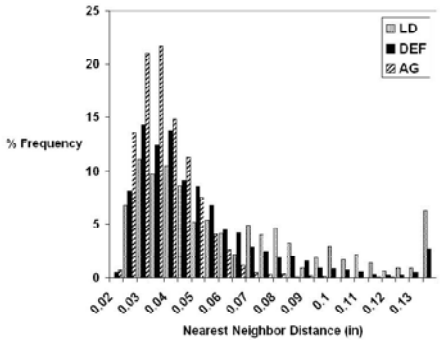


Figure 16 – Nearest Neighbor of tiles LD, DEF, and AG[10]

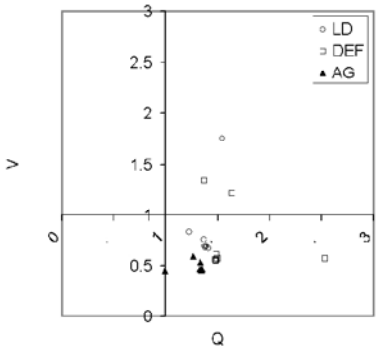


Figures 17 – Q-V plot of tiles LD, DEF, and AG[10]

The results from the ultrasound scans were divided into nine different amplitude ranges. Image analysis was performed for

each range to preserve the information in the data. Figure 16 displays the data from range 23-24mV, as it contained the most data points. A long tail can be seen for tile LD, and well as a large fraction of features with a nearest-neighbor distance greater than 0.14". The distribution for tile DEF also contains a tail, but it is not as pronounced as that for LD. The narrowest distribution is attributed to tile AG. Similar trends are maintained for the distributions of the remaining amplitude ranges[10].

A Q-V plot was also constructed that contained the data from the nine amplitude ranges, as shown in Figure 17. Most of the points fall into the region of Q>1 and V<1, which signifies a regular distribution. When a comparison is made to the Q-V plots obtained from microstructural analysis of the SEM micrographs, the results are inconclusive. However, the nearest neighbor distance distributions for the two methods do show a similar trend in that AG has the narrowest distribution, followed by DEF, and then LD.

Forty-one sintered SiC tiles comprise group III. The goal of this study is to determine if a correlation exists between mechanical properties, ultrasound evaluation, and ballistic performance.

The tiles have undergone non-destructive evaluation by ultrasound scanning with a 20 MHz transducer. This marks a departure from the previous ultrasound data presented above. As stated before, the ultrasound images that appear in Figure 15 were compiled using a 125 MHz transducer by recording the amplitude of the signal from the bottom surface reflection peak. An improvement of this technique includes a way to account for sample thickness, as the results from the bottom surface amplitude method can be affected by an uneven surface. For example, if both a thin and thick sample is scanned, the amplitude measured from the thin sample will be higher, even if the quality of both samples is considered to be the same. Furthermore, the measured amplitude will be severely affected by any surface perturbations or variations in how parallel the sample surfaces are.

In this study, the longitudinal wave time of flight, shear wave time of flight, and amplitude ratio of the 1st and 2nd bottom surface peaks were measured using a 20 MHz transducer. The longitudinal and shear time of flight information was used to produce a map of the Young's and shear moduli, while a map of the acoustic attenuation coefficient was calculated from the 1st and 2nd bottom surface peak amplitude information. This method was found to be preferable in comparison to measuring bottom surface amplitude as the measurement of the attenuation coefficient allows materials of different thicknesses to be compared. Additionally, the results are presented in the common unit of dB/cm. The utilization of a 20 MHz transducer provided sufficient acoustic energy for the shear wave peak to be resolved, which was not possible with the 125 MHz transducer available at the time of the measurement.

The first step in the measurement process is to accurately measure the thickness of the sample at every scanning point. Mode conversion of acoustic energy occurs at each surface, thereby converting some of the energy of the longitudinal wave into a transverse/shear wave. By measuring the longitudinal and shear wave time of flight, the longitudinal and shear velocity can be calculated according to $v = t \cdot d$. Poisson's ratio, Young's modulus, the shear modulus, and the acoustic attenuation coefficient can then be calculated at every scanning point according to the relationships defined by Brennan *et al*[11].

Ultrasound images for selected tiles in the series are shown in Figure 18. Based upon these results, the tiles were divided into six groups. Group headings include mean attenuation coefficient, high and low mean longitudinal velocity/Young's modulus, high and low mean shear velocity/shear modulus, and high and low zone variations.

One tile from each group will be sectioned

into MOR bars and broken under 4-pt loading. Before being broken, the Archimedes density of each bar will be measured, allowing a density map to be created for the respective tiles. This will give a proper indication of the density throughout the volume of the tile, as opposed to a bulk measurement. Knoop indentation testing and SEM microscopy will take place on the fractured bars. Finally, one tile from each group will undergo ballistic testing. It is expected that from the results of the mechanical and ultrasound testing a correlation will be made to the ballistic performance of the tiles. Results will be included in the future.

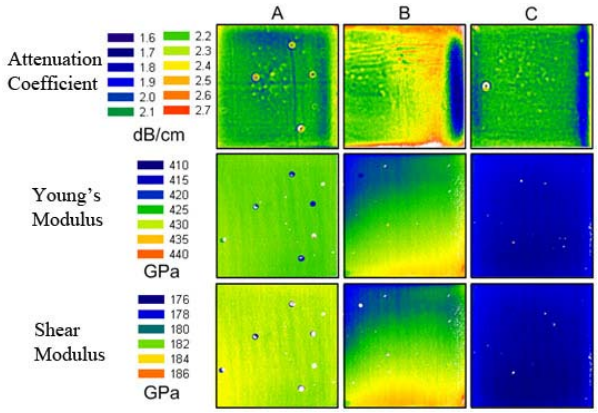


Figure 18 – Attenuation coefficient, Young's modulus, and shear modulus maps of sintered SiC tiles at 20 MHz[12]

## CONCLUSIONS

Three groups of commercially available SiC armor tiles were analyzed using various microstructural analysis tools, mechanical testing methods, and non-destructive evaluation techniques. The microstructural analysis methods included average pore size and pore size distribution, nearest-neighbor distribution, and Tessellation analysis. Mechanical testing was done using Knoop microhardness indentation to provide a comparison to the microstructural analysis results. The conclusions gained from this analysis are being applied to a new study, which will combine the previous methods with MOR testing and ballistic impact assessment of armor tiles. It is expected that non-destructive methods such as ultrasound C-scans will serve as a predictor of ballistic performance of armor ceramics.

## REFERENCES


[1]A.Tewari, A. M. Gokhale, "Nearest neighbor distances in uniaxial fiber composites", Computational Materials Science, 31 (2004) 13-23

[2]M.V. Demirbas, R.A. Haber, "Defining Microstructual Tolerance Limits of Defects for SiC Armor", Ceramic Armor and Armor Systems II, Ceramic Transactions, 178, p. 109-122, 2005

[3]D. Viechnicki, W. Blumenthal, M. Slavin, C. Tracy and H. Skeele, "Armor Ceramics – 1987", The Third Tacom Armor Coordinating Conference Proceedings

[4]John C. Russ, "Computer-Assisted Microscopy" 1990 Plenum Press, New York

[5]M. Berman, L. M. Bischof, E. J. Breen, G. M. Peden, "Image Analysis" *Materials Forum* 18, 1-19 (1994)

[6]J. P. Anson, J. E. Gruzlezski, "The Quantitative Discrimination between Shrinkage and Gas Microporosity in Cast Aluminum Alloys Using Spatial Data Analysis" *Materials Characterization* 43, 319-335 (1999)

[7]P. A. Karnezis, G. Durrant, B. Cantor, "Characterization of Reinforcement Distribution in Cast Al-Alloy/SiCp Composites" *Materials Characterization* 40, 97-109 (1998)

[8]N. Yang, J. Boselli, P. J. Gregson, I. Sinclair, "Simulation and Quantitative Assessment of Finite-size Particle Distributions in Metal Matrix Composites" *Materials Science and Technology* 16 (7-8): 797-805 JUL-AUG 2000

[9]A. M. Murphy, S. J. Howard, T. W. Clyne, "Characterization of severity of particle clustering and its effect on fracture of particulate MMCs" *Materials Science and Technology*, 14 (9-10):959-968 (1998)

[10]M.V. Demirbas, R.A. Haber, R.E. Brennan, "Spatial Distribution of Defects in Silicon Carbide and Its Correlation with Localized Property Measurements", (2007)

[11]R.E. Brennan, R.A. Haber, "Ultrasonic NonDestructive Evaluation of Armor Ceramics" Rutgers University Department of Materials Science and Engineering, Doctoral Thesis (2007)

[12]S. Bottiglieri, A. Portune, Rutgers University Department of Materials Science and Engineering (2008)